Design and Experimental Validation of a Multiband Conformal Patch Antenna for Animal Ingestible Bolus Applications

Said Benaissa, Denys Nikolayev, Günter Vermeeren, Kenneth Deprez,
Jasper Goethals, Bart Sonck, Frank A. M. Tuyttens, Luc Martens, David Plets, Wout Joseph

***Abstract*—Electronic boluses with biotelemetry capabilities enable wireless monitoring of animals' physiological data (e.g., temperature, pH). The aim of this study was to design and experimentally validate a novel multiband (434, 868, 1400) MHz conformal patch antenna for in-body biotelemetry applications for cows. The optimal frequency band was studied prior to the design of the antenna, based on the dielectric measurements of the antenna environment (i.e., rumen). The antenna was integrated in a 13.5 cm $\times \varnothing 3$ cm bolus and simulated in a $\varnothing 300$ mm spherical phantom with electromagnetic properties of cows' rumen fluid. The proposed antenna presented a high performance with a realized gain of (–38.5; –41.2; –45.7) dBi and a radiation efficiency of (0.012%; 0.0045%; 0.001%) at 434, 868, and 1400 MHz, respectively. Following the numerical analysis and optimization, a prototype was manufactured to experimentally evaluate the antenna performance. Good agreement was obtained between the measurements and simulations both for reflection coefficients and radiation performance. The measured gain was –36.3 dBi, –40.4 dBi, and –43.6 dBi, at 434, 868, and 1400 MHz, respectively. The proposed multiband antenna will enable the development of a new generation of boluses for animal biotelemetry applications to enhance the performance of the animal monitoring systems.**

***Index Terms*—Electronic bolus, in-body antenna, radiation efficiency, ruminal fluid, conformal patch antenna, cows, animal health monitoring, ISM (industrial, scientific, and medical) band, link budget.**

I. Introduction

SENSORS such as accelerometers, pedometers, and temperature sensors are being widely adopted by modern livestock farms for the collection and the interpretation of animal data [1]–[3]. Accurate interpretation of the sensors' data provides a profound insight into the health status, (re)productivity, and welfare of the animals [4]. In addition to on-body sensors (e.g., leg, or neck-mounted sensors), relevant data like pH and ruminal temperature are measured using in-body sensors integrated in ingestible boluses. Such data are used to increase the accuracy and the range of applications of the animal monitoring systems [5]. For example, a radio transmission rumen pH measurement system was developed and assessed in commercial dairy farms [6]. The use of radio-telemetric ruminal boluses to detect body temperature changes in dairy cattle is presented also in [7]. The measurement of the rumen temperature and acidity was used to estimate the health status of a cow's stomach with regard to acidosis, a known metabolic disorder of the cows' rumen after calving [8]. A review of the sensor technologies applicable to real-time monitoring of rumen environment was presented in [9]. These studies demonstrated the added value of electronic boluses for the monitoring of animal health and welfare. In addition, since the health and productivity of the animals are highly related to the health of the bacterial culture in the rumen, ruminant nutritionists have studied the digestive and fermentative processes of ruminant animals by leveraging fistulated cattle [9], [10]. Fistulation of an animal requires surgery and is only suitable for a limited number of research animals. By using electronic boluses, data could be collected continuously without surgery for a large number of animals.

The in-body devices rely on antennas to interface with external receivers. Existing animal telemetry systems mostly rely on canonical antenna designs that have been re-tuned (in terms of impedance) to operate in high-permittivity and lossy biological media. These antennas typically provide short-range (1–2 m) communication that can be improved by addressing the radiation efficiency [11]. In recent years, the understanding of antenna radiation in lossy finite-sized media has been substantially expanded [12]–[14]. Among others, these methodologies can help designers to choose the optimal design parameters – such as the antenna type and operating band – to improve the radiation performance. Better radiation characteristics would allow a longer range than 1–2 m, and would as such allow an automatic collection of in-body sensor data, instead of using a manual readout close to the animal body.

The reliability of the ingestible antenna is crucial for collecting accurate and real-time in-body data. For humans, several

This work was supported by the Research Foundation Flanders (FWO-V), Belgium. *(Corresponding author: Said Benaissa.)*

S. Benaissa, G. Vermeeren, K. Deprez, J. Goethal, L. Martens, D. Plets, and W. Joseph are with the Department of Information Technology, Ghent University/imec, iGent-Technologiepark 126, 9052 Ghent, Belgium (e-mail: wout.joseph@ugent.be)

S. Benaissa, F.A.M. Tuyttens, and B. Sonck are with Flanders Research Institute for Agriculture, Fisheries and Food (ILVO), Scheldeweg 68, 9090 Melle, Belgium (e-mail: bart.sonck@ilvo.vlaanderen.be)

D. Nikolayev is with the Univ Rennes, CNRS, Institut d'électronique et des technologies du numérique, UMR–6164, FR–35000 Rennes, France (e-mail: d@deniq.com).

F.A.M. Tuyttens is with the Department of Veterinary and Biosciences, Faculty of Veterinary Medicine, Ghent University, Heidestraat 19, B-9820 Merelbeke, Belgium

B. Sonck is with the Department of Animal Sciences and Aquatic Ecology, Faculty of Bioscience Engineering, Ghent University, Coupure links 653, B-9000 Ghent, Belgium

in-body antennas were proposed [15], [16]. For example, Shah *et al.* [17] proposed a dual band (915 MHz and 2.45 GHz) meandered line implantable antenna for intracranial pressure monitoring. This antenna has a volume of $8 \times 6 \times 0.5$ mm^3 and was encapsulated by a biocompatible shell of ceramic alumina. In another study [18], a multi-band (MedRadio, midfield, and three ISM bands) conformal implantable antenna was proposed. The antenna was integrated in a capsule system with a size 11×26 mm^2. The design consists of introducing meandered shaped slots with open ends in the antenna radiator and ground. The slots were responsible for a reduction in size, tuning to the desired frequencies, and bandwidth enhancement of the proposed antenna.

The proposed antennas for humans are small in size, because of the space constraints, and their performance is often not sufficient for large animals (e.g., cows, horses), due to the high in-to-out body path loss [19]. The aims and novelties of this work are to 1) design and 2) experimentally validate a multiband (434, 868, and 1400 MHz) conformal patch antenna for in-body applications for large animals (i.e., cows). A multiband antenna allows a wide range of IoT wireless technologies, while a conformal design dedicates most of the bolus volume to the circuitry, which enables more sensors and batteries to be integrated in the bolus. Consequently, it contributes to the further development of a new generation of animal boluses that involve a complex and dense integration of sensors, microcontrollers, and power sources. Therefore, a wide range of relevant data will be collected for an accurate monitoring of the health and welfare of cattle. This work was conducted in five consecutive steps: i) the study and selection of suitable operating frequencies; ii) the measurement of the dielectric properties of the antenna's surrounding environment (cow's rumen fluid); iii) the design of a conformal patch antenna within size constraints for the selected frequency bands (i.e., 434, 868, and 1400 MHz) and obtained dielectric properties; iv) evaluation of the performance of the designed antenna using dedicated EM software; and v) experimental validation of the obtained results using manufactured prototypes. As an application, we performed in-to-out body link budget analyses by using the performance of the proposed antenna and the results presented in [19].

II. Antenna Design Procedure

A. Selection of Operating Frequencies

The results of the studies presented in [12], [20] were used to select the optimal frequency bands. In [20], theoretical and realistic models to estimate the radiation efficiency of electric and magnetic sources in biological mediums were proposed. The sources were centered inside a spherical phantom with a predefined diameter (300 mm in this work, representing an average operating depth in cows) with dispersive dielectric properties (e.g., muscle-equivalent EM properties). As explained in [20], a spherical model provides useful results despite being only a rough approximation. Such a model introduces direction-independent losses conserving the intrinsic radiation pattern independently of the antenna orientation [20]. Therefore, it could serve as a reference, well-characterized phantom improving the reproducibility of the results and allowing to gauge antenna designs relatively to the maximum achievable efficiency for the established reference case.

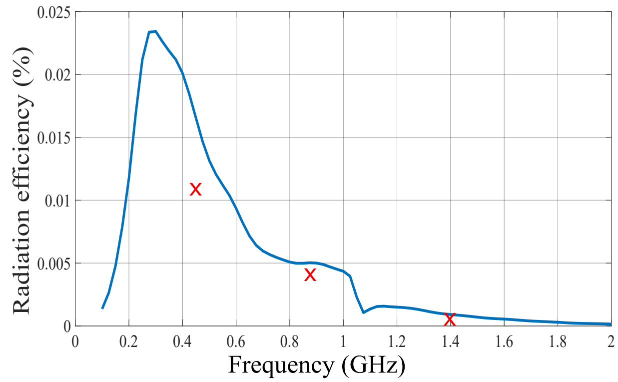

Fig. 1. The maximum achievable radiation efficiency of an equivalent transverse electric source in a spherical phantom with a diameter 300 mm with cow's rumen fluid electromagnetic properties (computed based on [12], [20]). The red marks are the simulated radiation efficiencies of the proposed antenna (Section III).

Calculations of the radiation efficiency were performed for an electric source with the same dimensions as the proposed antenna (see Section II-C) using a spherical phantom with a diameter of 300 mm and with the dielectric properties of a cow's rumen fluid (Section II-B). Fig. 1 shows the calculated radiation efficiency in percent as a function of the frequency. Considering both the deep-body application and the size of the animal, we chose to design the antenna for the 434, 868, and 1400 MHz ISM (Industrial, Scientific, and Medical) bands. These bands present lower power losses with optimal radiation efficiency values compared to the frequency bands above 1.4 GHz (Fig. 1). Conveniently, recent advances in low-power wireless communication technologies (e.g., Long Range (LoRa), Sigfox) working in the sub-GHz band (e.g., 434 MHz) allow long range wireless communications and are scalable towards a large number of devices. These technologies can be effectively used in health tracking of dairy cows, especially in large farms and in (remote) outdoor environments (pasture).

B. Electromagnetic Properties of Cow Ruminal Fluid

The radiation efficiency of a bolus located in the animal's rumen is paramount to improve both the operating range and power budget of the device. The antenna performance (in particular, the impedance matching) strongly depends on the electromagnetic properties of the surrounding environment, and impedance detuning results in the loss of total efficiency. Thus, the antenna must be optimized to perform optimally within a specified range of the dielectric properties.

The dielectric properties of a cow's rumen fluid were measured in the dairy barn of the Flanders Research Institute for Agriculture, Fisheries and Food (ILVO), Melle, Belgium. Fig. 2 shows the experimental setup. Three fistulated cows were used in this experiment. One liter of rumen fluid was extracted and put in a thermostat to keep it at a constant temperature (i.e., rumen temperature, $T = 36.5\ ^{\circ}C$). Dielectric properties i.e., relative permittivity (ε_r) and conductivity (σ)

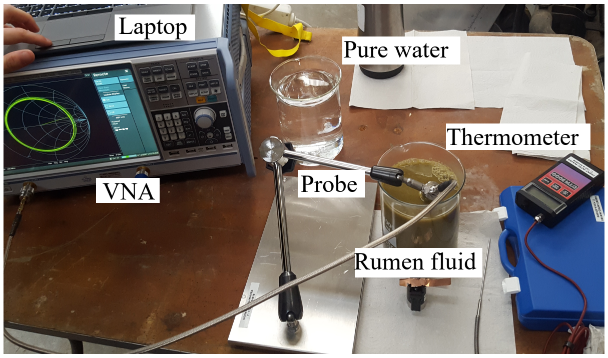

Fig. 2. Measurement setup for the dielectric properties of the cow's rumen fluid.

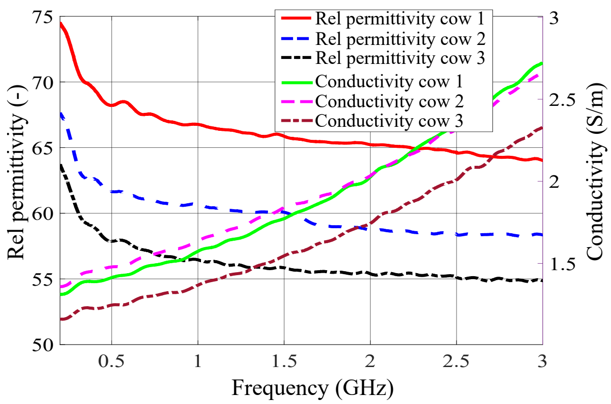

Fig. 3. The measured relative permittivity and conductivity of the rumen fluid for the three cows in the frequency band (0.2–3 GHz).

were measured in the 200-MHz-to-3-GHz band using a DAK-3.5 (Dielectric Assessment Kit) probe (Speag, Switzerland) in static conditions [21]. The data was processed with Speag software. The calculation of the EM properties is based on the open-ended coaxial probe transition method [22]. The measurements were repeated 10 times for each cow and the average values were considered.

Fig. 3 shows that there were differences between the three samples for both the relative permittivity and the conductivity (e.g., rumen fluid of cow 1 has higher permittivity than cows 2 and 3). This could be due to the difference in the rumen composition of the three cows. The standard deviation of the 10 repetitions was 0.04 S/m (2.1%) for the conductivity and 2.4 (3.3%) for the relative permittivity, meaning good repeatability. Table I summarizes the obtained results at 434, 868, and 1400 MHz. On average, the relative permittivity varied between 63.2 at 434 MHz and 60.6 at 1400 MHz. Similarly, the average conductivity varied between $\sigma = 1.3$ S/m at 434 MHz and $\sigma = 1.7$ S/m at 1400 MHz. These results were used as input to the antenna design and optimization procedure.

C. Antenna Design

Electronic boluses designed for cows have a cylindrical shape with a height of 130 to 145 mm and a diameter of 30 mm [6]. By using a flexible design that conforms to the

TABLE I
THE MEASURED RELATIVE PERMITTIVITY ε_r (-) AND CONDUCTIVITY σ (S/m) OF THE RUMEN FLUID FOR THE THREE COWS AT 434 MHz, 868 MHz, AND 1400 MHz ($T = 36.5\,°C$).

Freq (MHz)	**Cow 1**		**Cow 2**		**Cow 3**		**Average**	
	ε_r (-)	σ (S/m)	ε_r (-)	σ (S/m)	ε_r (-)	σ (S/m)	ε_r (-)	σ (S/m)
434	68.8	1.4	62.3	1.5	58.4	1.2	63.2	1.3
868	66.9	1.5	60.7	1.6	56.6	1.3	61.4	1.5
1400	65.9	1.7	60.1	1.8	55.8	1.5	60.6	1.7

shell of the bolus, the patch antenna can have maximum dimensions of 100 mm $\times$ 90 mm (i.e., $2\pi\times$ inner radius). We started the antenna design with a full rectangular patch antenna (step 1, Fig. 4a) with the maximum available space (100 mm $\times$ 90 mm). The initial antenna resonated at a single frequency of 927 MHz (Fig. 4d). To achieve lower resonance frequencies (with 434 MHz being the target one), different techniques can be used. A first option is the introduction of different types of slots [23], such as for example T-shaped, L-shaped, U-shaped, and Fork-shaped slots. The resonance frequencies are determined by the slot length and position [23]. The fractal method [24], [25] is a second approach to design multiband patch antennas. Fractals can be used in two ways to enhance antenna design [26]. The first method is the design of miniaturized antenna elements. The second method is to use the self-similarity in the geometry to blue print antennas, which are multiband or resonant over several frequency bands [26]. Besides using slots or fractals, other methods include the use of multilayer stacked antennas [23]. Most of these methods introduce a level of complexity in the antenna design leading to an increased cost and challenging integration in small devices. In this work, stair cuts were introduced on the radiating edges of the rectangular patch antenna to achieve resonance at lower frequencies (step 2, Fig. 4b). In step 3 (Fig. 4c), rectangular slots were introduced on the non-radiating edges of the patch to shift the resonance frequencies to the target frequencies (434, 868, and 1400 MHz). The introduced cuts create a discontinuity to make the electric current change its path along the ground plane and within the antenna [23]. This leads to an increase of the length of the electric current path, which impacts the input impedance at multiple operating bands. The optimized antenna design is shown in Fig. 4e. The antenna was designed for a flexible substrate RT/duroid 5880 ($\varepsilon_r = 2.2, \tan\,\delta = 0.0009$). After evaluating the mechanical stress due to folding to the target ⌀30 mm, the thickness of the substrate was set at 0.508 mm.

D. Numerical Analysis

The proposed antenna, wrapped inside the bolus (Fig. 4f) was modeled and simulated using the RF module of the COMSOL Multiphysics commercial computational package, version 6.0. The maximum finite element cell size used in any dielectric media was 0.1λ, where λ is the wavelength within that medium. The antenna and the substrate were meshed with 0.1 mm max step width. The excitation was provided by a

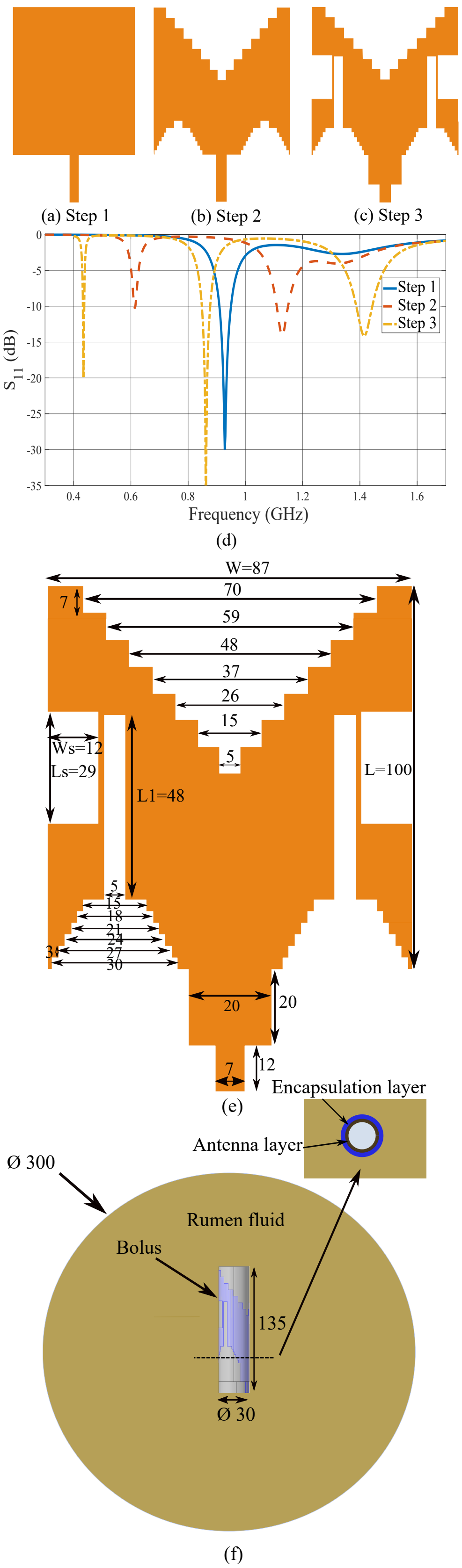

Fig. 4. Geometry and dimensions of the proposed antenna. (a-d) Design steps (e) Top view of the antenna with the optimized parameters. (f) Simulation setup in COMSOL Multiphysics software. All values are in mm.

voltage source of 1 V at the antenna terminal. An absorbing boundary condition followed by a perfectly matched layer was used at 0.5 m from the antenna. Increasing this distance had negligible effects.

The antenna was simulated inside a spherical homogeneous phantom (⌀300 mm representing the size of a cow's rumen, Fig. 4f). A spherical model of an animal body provides worthwhile and useful results despite being only a rough approximation. The spherical symmetry conserves the intrinsic radiation pattern of the antenna independently of its orientation, whereas other shapes (e.g., cylindrical or cubic) may lead to ambiguous representation of the antenna performance in terms of directivity. Moreover, it allows for comparing the antenna with counterparts. However, accurate evaluation of antenna radiation requires anatomical phantoms to account for the complex anatomy of the animal body. The frequency-dependent (dispersive) properties of the cow's rumen fluid were considered for the phantom. The antenna was matched to an impedance of 50 Ω. Simulations were run on a Dell server (Intel Xeon E5 2620). The bolus was filled with a biocompatible epoxy material with $\varepsilon_r = 3.2$ and $\tan\,\delta = 0.037$. Filling the capsule with such material helps preserving its structural integrity (i.e., electronics and circuitry). The antenna was encapsulated with a biocompatible material made of acrylic with dielectric properties ($\varepsilon_r = 2.01, \tan\,\delta = 0.001$). The antenna was optimized for an encapsulation layer with a thickness of 3 mm. A biocompatible insulation is required in the practical application of the bolus to avoid any adverse tissue reaction and to make the device isolated from the moist and corrosive environment of the rumen.

III. Antenna performance

A. *Reflection Coefficient*

Fig. 5 shows the impedance characteristics ($|S_{11}|$) of the antenna when computed in a phantom with EM properties of cows' rumen fluid. The difference between the three cows in terms of $|S_{11}|$ was small, especially at lower frequencies (434 and 868 MHz). For the 434 MHz-band, the resonance frequency f_{res} equaled 433.2 MHz and the –10 dB bandwidth BW was 10 MHz (Fractional bandwidth FBW = 2%). The resonance frequency for the 868 MHz-band was f_{res} = 862.4 MHz and the –10 dB BW was 30 MHz (FBW 3.4%). The available BW at 1400 MHz was higher than 434 MHz and 868 MHz bands, with a resonance frequency of f_{res} = 1418.1 MHz and –10 dB BW of 54 MHz (FBW 3.8%). The ISM bands at 434 MHz (433.05–434.79 MHz), 868 MHz (865–870 MHz), and 1400 MHz (1395–1400 MHz and 1427–1432 MHz) were fully covered for all cows separately and average dielectric values, as shown in Fig. 5.

B. *Radiation Performance*

Fig. 6 shows the radiation pattern of the antenna (azimuth and elevation) at 434, 868, and 1400 MHz inside the ⌀300 mm spherical phantom with EM properties of cow's rumen fluid (average). The radiation patterns at 434 MHz and 868 MHz are dipole-like, which is a desirable property for the in-to-out body communication. However, at 1400 MHz, the radiation

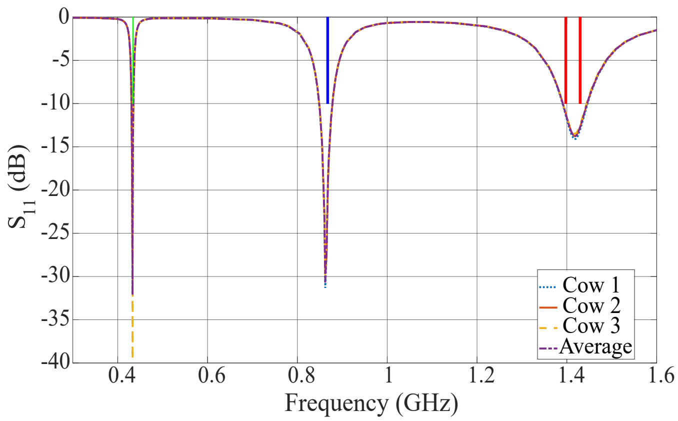

Fig. 5. Reflection coefficients of the conformal patch antenna simulated in a phantom with EM properties of cow's rumen fluid (3 cows and the average values in Table I). The green, blue, and red strips are the ISM bands at 434 MHz (433.05–434.79 MHz), 868 MHz (865–870 MHz), and 1400 MHz (1395–1400 MHz and 1427–1432 MHz), respectively.

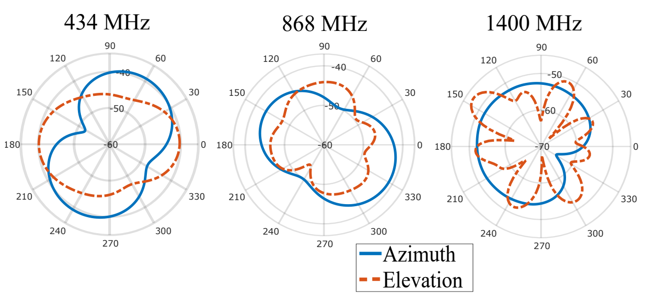

Fig. 6. Simulated radiation pattern. Realized gain (azimuth and elevation) of the patch antenna at (a) 434 MHz, (b) 868 MHz and (c) 1400 MHz simulated in ⌀300 mm phantom with EM properties of cow's rumen fluid.

pattern is directive with multiple lobes in the elevation plan. Table II lists the radiation characteristics of the antenna in terms of the gain (dBi), the radiation efficiency (%) and the realized gain (dBi) simulated in the ⌀300 mm spherical phantom with EM properties of cow's rumen fluid. The radiation efficiency was calculated using COMSOL software (i.e., the difference between accepted power by the antenna and the total radiated power). The highest gain was obtained at 434 MHz (–38.2 dBi). Similar values were obtained at 868 and 1400 MHz (–40.9 dBi and –45.7 dBi, respectively). We note that for the three frequencies, the cross-polarization gain was lower than the co-polarization gain with an average of –19 dB, –21 dB, –18 dB at 434, 868, and 1400 MHz, respectively. As expected, the highest radiation efficiency was obtained at 434 MHz (0.012%), followed by 868 MHz (0.0045%) and 1400 MHz (0.001%). These results agree well with the theoretical calculations (Section II-A). In addition, the obtained radiation efficiencies values are close to the maximum achievable values (0.016%, 0.005%, and 0.0015% for 434 MHz, 868 MHz, and 1400 MHz respectively).

C. Parametric Analysis

In this section a parametric study for antenna tuning is presented. The proposed antenna can be tuned to cover other frequency bands using the parameters Ws, L, Ls, and $L1$ (see

TABLE II
GAIN (dBi), RADIATION EFFICIENCY (%) AND REALIZED GAIN (dBi) OF THE CONFORMAL PATCH ANTENNA SIMULATED IN A ⌀300 mm SPHERICAL PHANTOM WITH EM PROPERTIES OF COW'S RUMEN FLUID.

Frequency (MHz)	**434**	**868**	**1400**
Gain (dBi)	–38.2	–40.9	–45.4
Radiation efficiency (%)	0.012	0.0045	0.001
Realized gain (dBi)	–38.5	–41.2	–45.7
Average Gain (dBi)	–45.2	–47.2	–55.7

Fig. 4e) The effect of the parameter Ws is presented in Fig. 7a. As shown, the variation of this parameter affected mainly the lower ISM band. Increasing the slot length shifted the lower ISM band from 434 MHz band to 402–405 MHz band (MICS). Fig. 7b shows the effects of varying the patch length L in the range of 94-100 mm. As expected, by decreasing L, the main resonance frequency was shifted from the 868 MHz band to the 915–928 MHz band, along with a negligible shift at the 434 and 1400 MHz. Finally, by increasing the parameter $L1$ and decreasing the parameter Ls, the resonance frequency at the higher band shifted from 1.3 GHz to 1.6 GHz (Fig. 7c). We note that a change of the parameter's values in the order of 0.1–0.2 mm has a negligible effect on the antenna performance. Consequently, the proposed antenna presents a high fabrication tolerance.

IV. Manufacturing and Experimental Validation

Following the numerical analysis and optimization, a prototype was manufactured to evaluate the antenna performance experimentally in the three considered bands.

A. Manufacturing Procedure

The antenna prototype was manufactured using laser ablation (LPKF ProtoLaser S) of 9 μm copper cladding on a 508-μm-thick Rogers RT/duroid 5880 substrate (see Fig. 8a). The printed design was soldered to a 100 mm 50 Ω coaxial cable terminated with an SMA connector. Then, the antenna was bent and inserted into a 135 mm ×⌀30 mm cylinder (see Fig. 8b). Similar to the numerical analysis, the antenna was encapsulated with a biocompatible plastic tube made of acrylic material ($\varepsilon_r = 2.01, \tan\delta = 0.001$) with a thickness of 3 mm. Epoxy was used to fill any remaining air gaps inside the bolus. A plastic tube was used to insulate the cable from the phantoms.

B. Preparation of Liquid Phantoms

To experimentally validate the antenna performance in terms of impedance and radiation, we prepared two liquid phantoms with rumen liquid equivalent properties (Section II-B). Several methods were proposed to achieve the target EM properties [27]. In this paper, we have chosen a water–sugar–salt formula [28]. Pure deionized water was used as a base component, sucrose to reduce the permittivity ε_r, and salt to increase the conductivity σ. The liquids were prepared in a 1 l container. A fixed quantity of water (800 ml) was used. A quantity of sugar (100 g) was first added. The salt is then added gradually (by 5 g) to the solution. The solution is kept for 5-10 min for

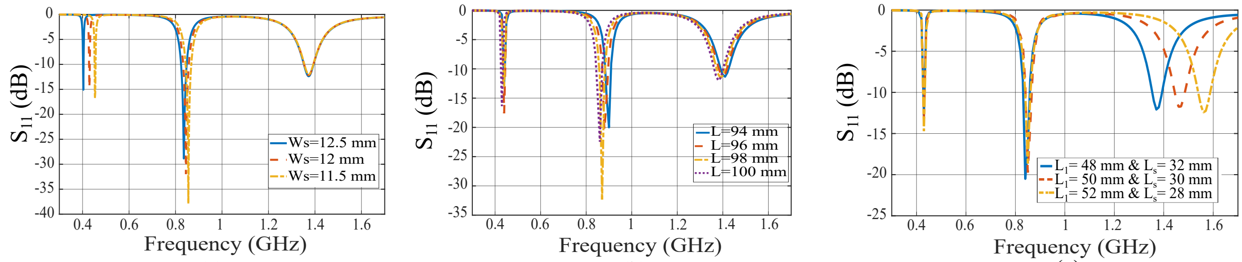

(a) (b) (c)

Fig. 7. Parametric study of the designed antenna. Influence of antenna parameters on antenna reflection coefficient $|S_{11}|$(dB) under different (a) Ws, (b) L, and (c) $L1$ and Ls.

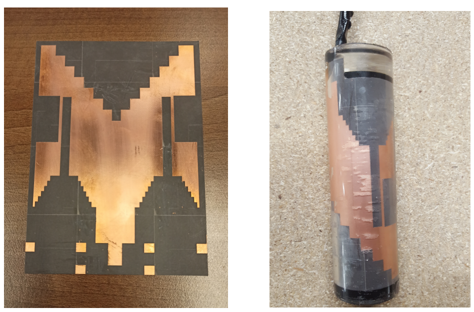

(a) (b)

Fig. 8. Bolus antenna prototype. (a) A Top view of the planar antenna. (b) Antenna soldered to a 50 Ω coaxial cable and warped in the 3-mm-thick encapsulation.

TABLE III
LIQUIDS USED FOR MEASUREMENTS: CONCENTRATIONS OF SUGAR C_{sugar} (g/mL) AND SALT C_{salt} (g/mL) WITH THE CORRESPONDING DIELECTRIC PROPERTIES AT 434 MHz AND 868 MHz (LIQUID 1, T = 22.5 °C) AND 1400 MHz (LIQUID 2, T = 22.2 °C).

	C_{sugar} **(g/mL)**	C_{salt} **(g/mL)**	**Freq (MHz)**	**Permittivity** ε_r **(-)**	**Conductivity** σ **(S/m)**
Liquid 1	0.750	0.054	434	64.6	1.25
			868	62.2	1.43
Liquid 2	0.337	0.022	1400	61.1	1.77

mixing (stirring using a magnetic). The relative permittivity and conductivity were then measured. The same procedure was repeated until the relative error between the final measured values and the target was less than 5%.

Table III lists the final optimal concentrations. The EM properties of the phantoms were measured using the SPEAG DAK kit with DAK-3.5 probe as explained in section II-B. The obtained permittivity and conductivity for liquid 1 (434 MHz and 868 MHz) and liquid 2 (1400 MHz) are listed in Table III. The difference between the measured and the target values is less than 3% for the permittivity and less than 5% for the conductivity.

C. Reflection Coefficient

The Rohde & Schwarz ZNB 20 (100 kHz–20 GHz) vector network analyzer (VNA) was used to measure the antenna reflection coefficient. The VNA was calibrated beforehand to remove the cable influence on the impedance. Fig. 9 shows the measured reflection coefficients for both liquid phantoms

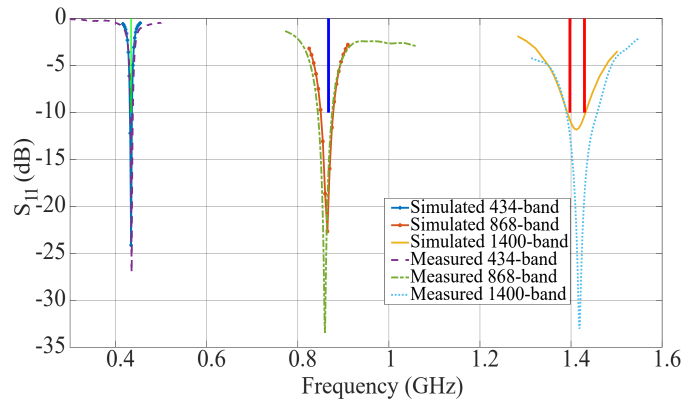

Fig. 9. Measured and simulated reflection coefficients $|S_{11}|$(dB) of the proposed antenna in the 200 mm × ⌀300 mm cylindrical glass container filled with the liquid 1 for 434 MHz and 868 MHz and with liquid 2 for 1400 MHz. The green, blue, and red strips are the ISM bands at 434 MHz (433.05-–434.79 MHz), 868 MHz (865-–870 MHz), and 1400 MHz (1395—1400 MHz and 1427-–1432 MHz), respectively.

with properties listed in Table III (liquid 1 for 434 MHz and 868 MHz bands and liquid 2 for 1400 MHz band). The experimental results agree very well with the simulations. As the substrate laser ablation provides lower precision than photolithography, even better agreement can be achieved using more precise manufacturing methods. The ISM bands at 434 MHz (433.05–434.79 MHz), 868 MHz (865–870MHz), and 1400 MHz (1395–1400 MHz and 1427–1432 MHz) were fully covered for both simulations and measurements.

D. Radiation Performance

The setup to measure the antenna gain is shown in Fig. 10. We used a 200 mm × ⌀300 mm cylindrical glass container filled with the prepared liquids. The antenna was placed at the center of the phantom. A rotation base (Maturo TT 0.8 PF) was used to accurately rotate the antenna and the phantom by a fixed angle (i.e., 5 degrees). The antenna was connected to the Rohde & Schwarz SMB100A (100 kHz–12.75 GHz) signal generator to inject a continuous wave signal with a constant power of 18 dBm at considered frequencies (434, 868, and 1400 MHz). The SRM-3006 probe (Narda, Germany) [29] was used as a receiver to record the received power. The probe was mounted at a height of 1 m using a plastic tripod. The probe was placed at a distance d = 3 m from the antenna fulfilling the far-field criterion $d \gg 2\lambda$. Absorbers were used to attenuate

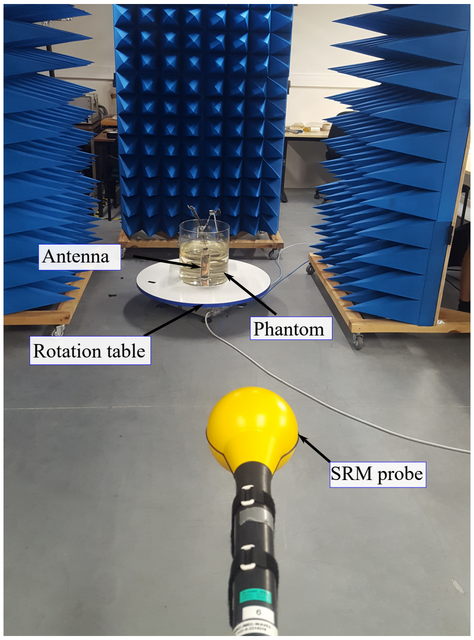

Fig. 10. Setup for the far-field characterization of the bolus antenna.

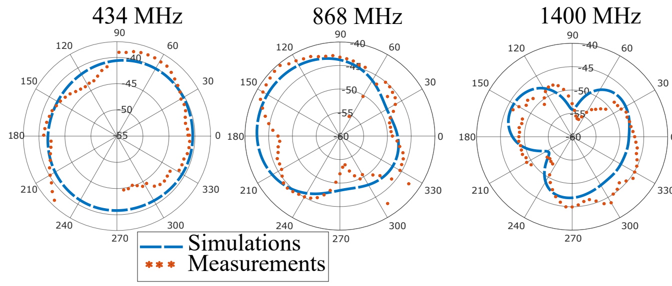

Fig. 11. Measured and simulated azimuthal gain (dBi) of the bolus antenna in the 200 mm × ⌀300 mm cylindrical glass container filled with the liquid 1 for 434 MHz and 868 MHz and with liquid 2 for 1400 MHz.

TABLE IV
SUMMARY OF THE MEASURED AND SIMULATED GAIN (dBi) OF THE BOLUS ANTENNA IN THE 200 mm × ⌀300 mm CYLINDRICAL GLASS CONTAINER FILLED WITH THE LIQUID 1 FOR 434 MHz AND 868 MHz AND WITH LIQUID 2 FOR 1400 MHz. *DIFFERENCE (MEASURED GAIN-SIMULATED GAIN).

Frequency (MHz)	**Max Gain (dBi)**		**Diff*** (dB)	**Avg Gain (dBi)**		**Diff*** (dB)
	Meas	Sim		Meas	Sim	
434	–36.3	–40.5	4.2	–40.7	–41.9	2.2
868	–40.4	–42.4	2.0	–44.6	–45.9	1.3
1400	–43.6	–45.6	2.0	–47.3	–48.7	1.4

reflected waves. We measured the radiation in the azimuth plane (elevation ϕ = 0°). The Friis formula was used to derive the realized gain from the measured data as explained in [30]–[32].

Fig. 11 shows the far-field characterization results. For the measured gain (maximum), –36.3 dBi, –40.4 dBi, and –43.6 dBi were obtained at 434 MHz, 868 MHz, and 1400 MHz respectively (Table IV). The highest difference between the measurements and the simulations was obtained at 434 MHz (4.2 dB). The difference was lower at 868 MHz and 1400 MHz (2 dB). On average, good agreement was obtained between the measured and simulated gain, with a difference of 2.2 dB, 1.3 dB, and 1.4 dB for 434 MHz, 868 MHz, and 1400 MHz respectively (Table IV). We note that there was a difference between the obtained radiation patterns in the measurements compared to the simulated ones in Fig. 6, especially at 1400 MHz. The radiation patterns in Fig. 6 were obtained using the spherical phantom with the measured EM properties of cow's rumen. However, the radiation patterns in Fig. 11 were obtained using a cylindric phantom with the EM properties of the prepared liquids. Some factors can explain the deviation between the two radiation patterns such as the reflections from the walls, since the room was not anechoic, the effect of the cables, and measurement errors.

V. Link Budget Analysis

A. In-to-out Body Signal-to-Noise Ratio

In this section, a link budget for an in-to-out body communication between the designed bolus placed in the cow's rumen and a distant receiving device was developed. Link budget analysis is essential to ensure a reliable transfer of the in-body data measured by the bolus. Under far–field conditions, we can calculate the link budget or, equivalently, the signal-to-noise ratio (SNR) at a receiving device (Rx). To calculate the SNR, the received power P_{Rx} (dBm) is calculated first using:

$$P_{\text{Rx}}\ (\text{dBm}) = P_{\text{Tx}} + G_{\text{Tx}} + G_{\text{Rx}} - \text{PL} \quad (1)$$

where P_{Tx} is the transmitter (Tx) power (dBm), G_{Tx} is the TX antenna gain (dBi), G_{Rx} = 2 dBi is the Rx antenna gain (a typical dipole antenna), and PL is the path loss (dB). In this paper, the Log-distance path loss model was adopted for the path loss calculation similar to [33], [34]. The Log-distance path loss model is a widely used empirical model for estimating signal attenuation in wireless communication systems. However, the model has several assumptions and limitations such as, homogeneous environment, isotropic antennas, and line of sight propagation. These assumptions and limitations can affect the accuracy of the model in in-body environments. These limitations were mitigated in this study by using the estimated signal attenuation (in-to-out body path loss) in real environments (barn). The Log-distance path loss is given by [33], [34]:

$$\text{PL}\ (\text{dB}) = 20\text{log}\left(\frac{4\pi d}{\lambda_0}\right) + 10n\text{log}\left(\frac{d}{d_0}\right) + M_s + M_f \quad (2)$$

where, λ_0 is the free space wavelength (m), n is the path loss exponent, d is the Tx–Rx distance (m), d_0 = 1 m is the reference distance [34], M_s is the shadowing margin, and M_s is the fading margin.

The shadowing margin (M_s) was determined such that 95% of the locations at coverage cell edge are covered by the wireless system. This margin was derived from the standard deviation around the path loss model ($\sigma_{\text{PL model}}$) and the standard deviation of the body loss ($\sigma_{\text{Body loss}}$) [19] and equals $1.65\sigma_{\text{tot}}$, with $\sigma_{\text{tot}} = \sqrt{\sigma^2_{\text{PL model}} + \sigma^2_{\text{Body loss}}}$. Based on [19], a shadowing margin of 5.2 dB was considered. A Fade margin

TABLE V
DISTANCE (M) AT SNR =0 dB FOR THE CONSIDERED SCENARIOS. LOS (n = 1.5), NLOS (n = 3).

	Scenarios			
Frequency (MHz)	$G_{\text{Tx, max}}$ LOS	$G_{\text{Tx, max}}$ NLOS	$G_{\text{Tx, avg}}$ LOS	$G_{\text{Tx, avg}}$ NLOS
434	15.5	7.2	12.5	5.7
868	8.0	4.5	5.6	3.3
1400	5.2	3.1	4.0	2.7

(M_f) of 6 dB was considered for an outage probability of 0.01 (99% of the time, the variation around the median will not exceed the fade margin) [34].

The SNR (dB) is then calculate using the received power P_{Rx} and the total power of background noise P_{noise} as follows:

$$\text{SNR (dB)} = P_{\text{Rx}} - P_{\text{noise}} \quad (3)$$

In this paper, the measured noise power in our previous study [19] (P_{noise} = –95 dBm) was considered. This value is used for the SNR calculation. The noise power was measured for a bandwidth of 3 MHz, which is higher than the RF signal bandwidth of IoT wireless technologies (e.g., 0.5 MHz for LoRa, 1 MHz for BLE, 0.6 MHz for Zigbee, and 0.2 MHz for NB-IoT). Moreover, the presented SNR plots as a function of Tx–Rx distance (Fig. 12) can be used to deduce the wireless range for different noise power values. For each frequency band, four communication scenarios were considered: optimal line-of-sight LOS (max gain $G_{\text{Tx, max}}$, n = 1.5), optimal NLOS ($G_{\text{Tx, max}}$, n = 3), average LOS ($G_{\text{Tx, avg}}$, n = 1.5), average NLOS ($G_{\text{Tx, avg}}$, n = 3). Fig. 12(a–c) shows the SNR as a function of Tx–Rx distance for the considered scenarios at 434, 868 and 1400 MHz. A horizontal line at 0 dB was plotted to show the distance corresponding to an SNR = 0 dB (the power of the received signal equals to the noise power). In most wireless communication schemes, the received power should be higher than the noise power for a correct demodulation. As shown in Fig. 12, the SNR decreases as a function of the Tx–Rx distance, due to the decrease of the received power. At 434 MHz, SNR = 0 dB corresponds to higher distances than 868 and 1400 Hz. This means that 434 MHz allows higher TX–Rx distances than 868 MHz and 1400 MHz. Table V lists the distance (m) for an SNR = 0 dB. At 434 MHz, The distance varied between 15.5 m and 5.7 m (worst case). As expected, lower values were obtained at 868 MHz and 1400 MHz. However, the available bandwidth at 434 MHz is much lower than 868 or 1400 MHz. In fact, there is a trade-off between the available bandwidth and communication range. Consequently, the proposed antenna can be used for different applications depending on the required data rate and network range.

B. Application: LoRa network range

As application, LoRa technology is proposed for in-body data collection for dairy cows accounting for the bolus antenna gain. The LoRa physical layer protocols enables us with low-power and long-distance communications through Chirp Spread Spectrum modulation [35], [36]. Other advantages of LoRa over other low-power wide-area network technologies

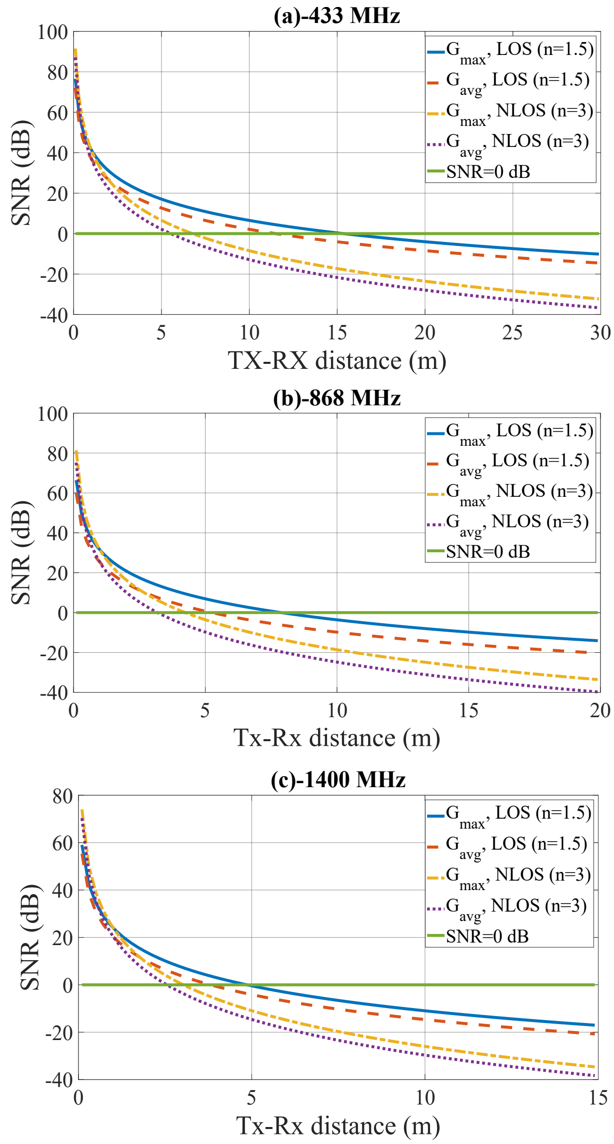

Fig. 12. SNR (dB) a as function of the Tx–Rx distance (m) for the considered scenarios at (a) 434 MHz, (b) 868 MHz, and (c) 1400 MHz.

are the open-source MAC protocol (i.e., LoRaWAN) specification, low-cost application availability, and community support [37]. LoRa technology can demodulate signals with an SNR lower than 0 dB [37]. Consequently, the network range can be extended significantly.

Based on the calculated SNR values at 868 MHz (Fig. 12b), the wireless range of a LoRa network is calculated for different data rates. Each data rate (i.e., bitrate) requires a certain SNR value [38], with higher data rates require higher SNR values [38]. Table VI lists the obtained wireless range for the worst-case scenario (minimum) and optimal scenario (maximum). The minimum range varied between 4.6 m and 8.2 m and the maximum range varied between 13.5 m and 32.4 m for the higher and lower data rate, respectively. These network ranges will allow reliable data collection of in-body date and enable real-time tracking of the cows' health and welfare.

TABLE VI
MAXIMUM AND MINIMUM LORA NETWORK RANGE USED FOR IN-TO-OUT BODY DATA COLLECTION FOR COWS. SF: SPREADING FACTOR.

Bitrate	**SF**	**SNR**	**Range (m)**	
(bps)	(-)	(dB)	Min	Max
5469	7	-7.5	4.6	13.5
3125	8	-10	5.0	15.2
1758	9	-12.5	5.4	18.6
977	10	-15	6.5	21.3
537	11	-17.5	7.3	25.7
293	12	-20	8.2	32.4

VI. DISCUSSION

In this paper, a new conformal multiband patch antenna for animal ingestible bolus applications was designed and experimentally validated. The proposed multiband antenna for animal biotelemetry applications is, to the best of our knowledge, the first of its kind that enables development of a new generation of animal boluses.

We started the antenna design by selecting the optimal frequency band based on the theoretical maximum achievable radiation efficiency in a spherical phantom of a diameter 300 mm with cow's rumen fluid dielectric properties. The antenna was designed to operate at the free ISM bands i.e., 434 MHz, 868 MHz, and 1400 MHz. The availability of these three bands enlarges the possible applications of the bolus. A lower frequency band (e.g., 434 MHz) can be used to reach longer ranges with limited data rates, while higher frequency bands (e.g., 868 and 1400 MHz) can be used to transmit at higher data rates. In addition to the radiation efficiency and body attenuation, the selection of the frequency band for deep-body communication depends on the required data rate, power consumption, and communication range. In general, higher data rates require wider bandwidths, which can be difficult to achieve in high density barns due to the limited available bandwidth and potential interference. Higher power consumption can also cause heating of the surrounding tissue, which can be harmful to the animal. The communication range is also limited by the attenuation of the signals by the metallic construction in the cow barn. The use of a biocompatible plastic encapsulation and epoxy filling, highly reduces the manufacturing costs, compared to antennas with ceramic capsule shell and a high-permittivity filling [39]. A cost-effective antenna is required, especially for applications in farms with large herds.

The reflection coefficient of the proposed antenna was evaluated in three cow rumen fluid samples. Although the EM properties of the three samples varied considerably (conductivity range 1.2–1.5 S/m and relative permittivity range 58.4–68.8, at 434 MHz), the reflection coefficient of the antenna did not change significantly. This reflects the robustness of the antenna and its applicability for other cows. This antenna may also be considered for other animals (e.g., horses), since the EM properties of animal tissues are similar [40]. Moreover, the robustness of the antenna reduces partially the impedance detuning.

The obtained radiation performance (gain and efficiency) of the proposed antenna was lower compared to in-body antennas for humans [41]–[44] (see Table VII). As reported in [45], ingestible antennas for humans have a realized gain between –22 dBi and –37 dBi. Although these antennas have smaller size (a length between 17–32 mm and a diameter of 7–11 mm), they are simulated in much smaller phantom size (generally a sphere of ⌀100 mm) compared to a sphere of ⌀300 mm representing a cow's rumen (27 times smaller in volume). Moreover, since the available space in implanted devices used for humans is limited, several miniaturization techniques were proposed [46]. Antenna miniaturization consists mainly of two approaches: extending the current flow path and using high-permittivity substrate materials [46]. For example, Basir *et al.* [47] increased the current path and minimized the antenna by using slot technology and symmetric structure with a thin polyamide substrate ($\varepsilon_r = 4.3, \tan\,\delta = 0.004$) to save space. In Liu *et al.* [48], double spiral arms were employed to expand the effective current path to achieve miniaturization of a hemispherical conformal antenna. In Li and Guo [49], a slot dual-polarized capsule antenna was designed using a stepped slot and a symmetrical structure to reduce the antenna size. Nguyen *et al.* [50] proposed a miniaturized implantable antenna for biomedical applications. The miniaturization of the proposed antenna was obtained by using two pairs of a rectangle slots and a meander line as radiating patch. These miniaturization techniques are suitable alternative approaches to design antennas for small ruminants, such as goats and sheep.

The proposed antennas for humans present some limitations for animal in-body applications. For example, because of the space constraints, the proposed antennas for humans are small in size and their performance is often not sufficient for large animals (e.g., cows, horses), due to the high in-to-out body path loss. Moreover, as explained, most of these antennas are miniaturized. The miniaturization techniques often led to a reduction in efficiency and gain, especially when immersed in lossy surrounding tissue [57]. Finally, tuning miniaturized antennas to other applications can be challenging due to their small size, and it may be difficult to achieve the desired requirements.

In-body antennas with circular polarization were proposed to reduce the effect of multipath reflections caused by the human body. However, based on the findings presented in [58], circular polarization does not show substantial advantage over the linear one for in-body applications. Moreover, the polarization loss can be recovered at off-body receiver side using dual-polarized antennas and, therefore, simplify the design of the space-constrained in-body antennas.

The antenna has been simulated and experimentally tested in homogeneous in-body environments. In practice, the animal rumen is highly anisotropic and heterogeneous. As stated in [39], the radiation of in-body antennas is significantly affected by heterogeneity [39]. The obtained values of the antenna gain and efficiency using a spherical/cylindrical phantom allow for comparing the antenna with counterparts. Accurate evaluation of antenna radiation for any particular scenario requires a statistical-EM approach anatomical phantoms.

Finally, the antenna is matched for a standard input impedance of 50 Ω for the three bands. It contributes to the

TABLE VII
COMPARISON OF THE MULTIBAND IN-BODY IMPLANTABLE ANTENNAS REPORTED IN THE LITERATURE.

Litt.	**Year**	**Freq.** (MHz)	**Size** (mm) **Antenna**	**Capsule**	**Phantom Type**	**Size** (mm)	**BW** (MHz)	**Gain** (dBi)
[44]	2011	403 2450	32.1×10	$32.1 \times \varnothing 5.1$	Cylinder	80×110	10 130	–28.8 –18.5
[46]	2017	403 915 2450	$29.8 \times 14 \times 0.2$	$25 \times \varnothing 11$	Cuboid	$100 \times 100 \times 110$	47 85 487	–29.7 –24.9 –23.2
[17]	2018	915 2450	$8 \times 6 \times 0.5$	$15 \times 7 \times 3.45$	Cube	200^3	90 210	–28.5 –22.8
[47]	2020	915 2450	$32 \times 10 \times 0.025$	$26 \times \varnothing 11$	Cube	200^3	104 55	–28.7 –20.8
[51]	2020	403 2450	$18 \times 10 \times 0.1$	$16 \times \varnothing 6$	Cuboid	$50 \times 100 \times 100$	236 2670	–29.7 –25.4
[18]	2020	402 915 1200	$19 \times 15 \times 0.2$	$26 \times \varnothing 11$	Cuboid	$20 \times 100 \times 100$	155 180 97	–30.8 –19.7 –18.7
[52]	2021	915 2450	$6.5 \times 6.5 \times 0.5$	$26 \times \varnothing 11$	Cube	100^3	124 154	–28.2 –24.5
[53]	2022	414 2400 5700	$12 \times 12 \times 1.4$	–	Skin	50×50	53 90 300	–45.0 –18.0 –14.0
[54]	2022	434 2450	20×19	$25 \times \varnothing 7$	Sphere	$\varnothing 100$	42 535	–28.9 –18.6
[55]	2022	433 915 2450	$15 \times 15 \times 1.2$	–	Cuboid	$7.4 \times 95 \times 95$	82 162 758	–33.8 –16.8 –21.2
[56]	2023	2400 4800 5800	$9.2 \times 9.2 \times 0.5$	$15 \times 10 \times 3$	Skin	$42 \times 100 \times 100$	150 75 200	–15.2 –16.6 –15.8
[57]	2023	860 1850 2450	$10 \times 10 \times 1.1$	–	Cuboid	$45 \times 130 \times 130$	134 138 458	–31.8 –21.8 –18.5
This work	–	434 868 1400	$87 \times 132 \times 0.5$	$135 \times \varnothing 30$	Sphere	$\varnothing 300$	10 30 54	–38.5 –41.2 –45.7

further development of a new generation of animal boluses that involve a complex and dense integration of sensors, microcontrollers, and power sources.

VII. CONCLUSION

This paper presented the design and the experimental validation of a novel multiband (434, 868, 1400) MHz conformal patch antenna for in-body biotelemetry applications for cows. The proposed antenna has a realized gain of (–38.5; –41.2; –45.7) dBi and a radiation efficiency of (0.012%; 0.0045%; 0.001%) at 434, 868, and 1400 MHz, respectively, when simulated in a spherical phantom with a diameter of 300 mm. Good agreement was obtained between the measurements and simulations for both reflection coefficients and radiation performance. The measured gain was –36.3 dBi (434 MHz), –40.4 dBi (868 MHz), and –43.6 dBi (1400 MHz), with a difference between measurements and simulations of 2.2 dB (434 MHz), 1.3 dB (868 MHz), and 1.4 dB (1400 MHz). LoRa technology was proposed for in-body data collection for cows, which enables network ranges up to 32 m.

In future work, measurement with designed antenna will be performed to evaluate the wireless range in real environments (barn) with fistulated cows. The measurement of the wireless propagation in these scenarios allows accurate characterization of the in-to-out body communication. Future work will also consider the integration of a PCB with sensors (accelerometer, temperature sensor) in the bolus. The success of the bolus will enable collecting reliable in-body data for a wide range of applications (accelerometer, temperature, pH, endoscopic imagery, etc.). These data will consequently contribute to the accurate tracking and monitoring of cows' health and welfare.

ACKNOWLEDGMENT

The authors would like to thank Leen Vandaele and Dirk Langerock for their help during the measurements. Said Benaissa is a Post-Doctoral Fellow of the FWO-V (Research Foundation Flanders, Belgium).

REFERENCES

[1] E. P. Romanzini, R. N. Watanabe, N. V. B. Fonseca, A. S. Berça, T. R. Brito, P. A. Bernardes, D. P. M., and R. A. Reis , "Modern livestock farming under tropical conditions using sensors in grazing systems," *Sci. Rep.*, vol. 12, 2654, 2022.

[2] M. J. O'Grady and G. M. P. O'Hare, "Modelling the smart farm," *Inf. Process. Agric.*, vol. 4, no. 3, pp. 179–187, 2017.

[3] S.Morrone, C. Dimauro, F.Gambella, and M.G. Cappai, "Industry 4.0 and precision livestock farming (PLF): an up to date overview across animal productions," *Sensors*, vol. 22, no. 12, 4319, 2022.

[4] S. Benaissa, F.A.M. Tuyttens, D. Plets, T. de Pessemier, J. Trogh, E. Tanghe, , L.Martens, L.Vandaele, A. Van Nuffel, W. Joseph, and B. Sonck, "On the use of on-cow accelerometers for the classification of behaviours in dairy barns," *Res. Vet. Sci.*, pp. 425–433, 2019.

[5] I. Eihvalde, D. Kairisa, and I. Sematovica, "Long-term continuous monitoring of ruminal pH and temperature for dairy cows with indwelling and wireless data transmitting unit," in *Engineering for Rural Development*, ERD, 2016, vol. 2016–Jan, pp. 726–731.

[6] S. Sato, H. Mizuguchi, K. Ito, K. Ikuta, A. Kimura, and K. Okada, "Technical note: Development and testing of a radio transmission pH measurement system for continuous monitoring of ruminal pH in cows," *Prev. Vet. Med.*, vol. 103, no. 4, pp. 274–279, 2012.

[7] O. Alzahal, H. Alzahal, M. A. Steele, M. Van Schaik, I. Kyriazakis, T. F. Duffield, and B. W. McBride, "The use of a radiotelemetric ruminal bolus to detect body temperature changes in lactating dairy cattle," *J. Dairy Sci.*, vol. 94, no. 7, pp. 3568–3574, 2011.

[8] R. Antanaitis, V. Žilaitis, V. Juozaitiene, and R. Stoškus, "Usefulness of acidity and temperature of the rumen and Abomasum in Diagnosing SARA in Dairy Cows after Calving," *Pol. J. Vet. Sci.*, vol. 19, no. 3, pp. 553–558, 2016.

[9] C. S. Han, U. Kaur, H. Bai, B. Roqueto dos Reis, R. White, R. A. Nawrocki, R. M. Voyles, M. G. Kang, and S. Priya, "Invited review: Sensor technologies for real-time monitoring of the rumen environment," *J. Dairy Sci.*, vol. 105, pp. 6379–6404, Jun 2022, doi: 10.3168/jds.2021-20576.

[10] T. Mottram, J. Lowe, M. McGowan, and N. Phillips, "Technical note: A wireless telemetric method of monitoring clinical acidosis in dairy cows," *Comput. Electron. Agric.*, vol. 64, no. 1, pp. 45–48, 2008.

[11] D. Nikolayev, M. Zhadobov, P. Karban, and R. Sauleau, "Conformal antennas for miniature in-body devices: the quest to improve radiation performance," *URSI Radio Science Bulletin*, vol. 2017, no. 363, pp. 52–64, 2017.

[12] D. Nikolayev, M. Zhadobov, P. Karban, and R. Sauleau, "Electromagnetic radiation efficiency of body-implanted devices," *Phys. Rev. Appl.*, vol. 9, no. 2, p. 24033, 2018.

[13] A. K. Skrivervik, M. Bosiljevac, and Z. Sipus, "Fundamental limits for implanted antennas: Maximum power density reaching free space," *IEEE Trans. Antennas Propag.*, vol. 67, no. 8, pp. 4978–4988, 2019.

[14] M. S. Mirmoosa, S. Nordebo, and S. A. Tretyakov, "Physical meaning of the dipole radiation resistance in lossless and lossy media: what is the radiation resistance of antennas in lossy media," *IEEE Antennas Propag. Mag.*, vol. 62, no. 4, pp. 75–81, 2020.

[15] T. M. Neebha, A. D. Andrushia, and S. Durga, "A state-of-art review on antenna designs for ingestible application," *Electromagn. Biol. Med.*, vol. 39, no. 4, pp. 387–402, 2020.

[16] M. M. Soliman, M. E. H. Chowdhury, A. Khandakar, M. T. Islam, Y. Qiblawey, F. Musharavati, and E. Zal Nezhad, "Review on Medical Implantable Antenna Technology and Imminent Research Challenges," *Sensors*, vol. 21, pp. 3163, May 2021, doi: 10.3390/s21093163.

[17] S. A. A. Shah and H. Yoo, "Scalp-implantable antenna systems for intracranial pressure monitoring," *IEEE Trans. Antennas Propag.*, vol. 66, no. 4, pp. 2170–2173, Apr. 2018.

[18] M. Yousaf, I. B. Mabrouk, F. Faisal, M. Zada, Z. Bashir, A. Akram, M. Nedil, and H. Yoo, "Compacted conformal implantable antenna with multitasking capabilities for ingestible capsule endoscope," *IEEE Access*, vol. 8, pp. 157617–157627, 2020, doi: 10.1109/ACCESS.2020.3019663

[19] S. Benaissa, L. Verloock, D. Nikolayev, M. Deruyck, G. Vermeeren, L. Martens, F.A.M. Tuyttens, B. Sonck, D. Plets, and W. Joseph, "Propagation-loss characterization for livestock implantables at (433, 868, 1400) MHz," *IEEE Trans. Antennas Propag.*, vol. 69, no. 8, pp. 5166–5170, 2021.

[20] D. Nikolayev, W. Joseph, M. Zhadobov, R. Sauleau, and L. Martens, "Optimal radiation of body-implanted capsules," *Phys. Rev. Lett.*, vol. 122, no. 10, p. 108101, 2019.

[21] SPEAG. *Dielectric Assessment Kit*. Accessed: Nov. 22, 2022. [Online]. Available: http://www.speag.com/products/dak/

[22] W. J. Ellison and J. -M. Moreau, "Open-Ended Coaxial Probe: Model Limitations," *IEEE Transactions on Instrumentation and Measurement*, vol. 57, no. 9, pp. 1984–1991, Sept. 2008, doi: 10.1109/TIM.2008.917683.

[23] G. Li and M. Li, Broadband microstrip antenna array, vol. 26, no. 6. 1998.

[24] D. H. Werner, R. L. Haupt, and P. L. Werner, "Fractal antenna engineering: the theory and design of fractal antenna arrays," *IEEE Antennas Propag. Mag.*, vol. 41, no. 5, pp. 37–58, 1999.

[25] D. H. Werner and S. Ganguly, "An overview of fractal antenna engineering research," *IEEE Antennas Propag. Mag.*, vol. 45, no. 1, pp. 38–57, 2003.

[26] B. Biswas, A. Karmakar, and V. Chandra, "Fractal inspired miniaturized wideband ingestible antenna for wireless capsule endoscopy," *AEU - Int. J. Electron. Commun.*, vol. 120, p. 153192, 2020.

[27] P. S. Hall and Y. Hao, *Antennas and propagation for body-centric wireless communications*, 2nd ed. Norwood, MA, USA: Artech House, 2012.

[28] T. Karacolak, A. Hood, and E. Topsakal, "Design of a dual-band implantable antenna and development of skin mimicking gels for continuous glucose monitoring," *IEEE Trans. Microw. Theory Techn.*, vol. 56, no. 4, pp. 1001–1008, Apr. 2008.

[29] M. Meisenburg,*SRM-3006, field strength analyzer*, Accessed: Nov. 22, 2022. [Online]. Available: www.narda-sts.com/en/selective-emf/srm-3006-field-strength-analyzer/srm-3006-3006101

[30] Balanis, C.A.,"Fundamental parameters and figures-of-merit of antennas," in *Antenna theory analysis and design*, New Jersey, 2016, John Wiley & Sons Inc., vol. 4, pp. 101–103.

[31] J. Li, Z. Kesheng, W. Weilong and L. Xiao, "The correction of antenna factor," in *International Symposium on Electromagnetic Compatibility*, Qingdao, Oct. 2007, pp. 524–527, doi: 10.1109/ELMAGC.2007.4413546.

[32] MORAN, M. "Electronic warfare and radar systems - Engineering Handbook," *US Naval Air Warfare Center Weapons Division*, p. 192, 2013.

[33] E. Reusens, W. Joseph, B. Latre, B. Braem, G. Vermeeren, E. Tanghe, L. Martens, C. Blondia, and I. Moerman, "Characterization of on-body communication channel and energy efficient topology design for wireless body area networks," *IEEE Trans. Inf. Technol. Biomed.*, vol. 13, pp. 933–945. 2009.

[34] S. Benaissa, D. Plets, E. Tanghe, J. Trogh, L. Martens, L. Vandaele, L. Verloock, F.A.M. Tuyttens, B. Sonck, and W. Joseph, "Internet of animals: characterisation of LoRa sub-GHz off-body wireless channel in dairy barns," *Electron. Lett.*, vol. 53, pp. 1281–1283, 2017.

[35] M.I.Z. Azhar Muzafar, A. Mohd Ali, and S. Zulkifli, "A study on LoRa SX1276 performance in IoT health monitoring", *Wirel. Commun. Mob. Comput.*, vol. 2022, p. 6066354, 2022.

[36] A. Zourmand, A. L. Kun Hing, C. Wai Hung, and M. Abdulrehman, "Internet of things (IoT) using LoRa technology," in *IEEE International Conference on Automatic Control and Intelligent Systems, I2CACIS*, Selangor, Malaysia, Jun. 2019, pp. 324–330.

[37] E. Sallum, N. Pereira, M. Alves, and M.Santos, "Improving quality-Of-service in LoRa low-power wide-area networks through optimized radio resource management", *J. Sens. Actuator Netw*, vol. 9, 2020.

[38] Committee, L.A.T. *LoRaWAN 1.1 Specification*. LoRa Alliance Stand 2017, 1. . Accessed: Dec. 1, 2022. [Online]. https://lora-alliance.org/wp-content/uploads/2020/11/lorawantm_specification_-v1.1.pdf

[39] D. Nikolayev, M. Zhadobov, and R. Sauleau, "Immune-to-detuning wireless in–body platform for versatile biotelemetry applications," *IEEE Trans. Biomed. Circuits Syst.*, vol. 13, no. 2, pp. 403–412, 2019.

[40] M.A. Stuchly, T.W. Athey, S.S. Stuchly, G.M. Samaras, and G. Taylor, "Dielectric properties of animal tissues in vivo at frequencies 10 MHz–1 GHz," *Bioelectromagnetics*, vol. 2, pp. 93–103, 1981.

[41] L.J. Xu, Y.X. Guo, and W. Wu, "Bandwidth enhancement of an implantable antenna," *IEEE Antennas Wirel. Propag. Lett.*, vol. 14, pp. 1510–1513, 2015.

[42] R. S. Alrawashdeh, Y. Huang, M. Kod, and A. A. B. Sajak, "A broadband flexible implantable loop antenna with complementary split ring resonators," *IEEE Antennas Wirel. Propag. Lett.*, vol. 14, pp. 1506–1509, 2015.

[43] C. Liu, Y.-X. Guo, and S. Xiao, "Circularly polarized helical antenna for ISM–band ingestible capsule endoscope systems," *IEEE Trans. Antennas Propag.*, vol. 62, no. 12, pp. 6027–6039, 2014.

[44] F. Merli, L. Bolomey, J. Zurcher, G. Corradini, E. Meurville, and A. K. Skrivervik, "Design, realization and measurements of a miniature antenna for implantable wireless communication systems," *IEEE Trans. Antennas Propag.*, vol. 59, no. 10, pp. 3544–3555, Oct. 2011.

[45] D. Nikolayev, M. Zhadobov, L. Le Coq, P. Karban, and R. Sauleau, "Robust ultra-miniature capsule antenna for ingestible and implantable applications," *IEEE Trans. Antennas Propag.*, vol. 65, no. 11, pp. 6107–6119, Nov. 2017.

[46] Z. Bao, Y. X. Guo, and R. Mittra, "Single-layer dual-/tri-band inverted-F antennas for conformal capsule type of applications," *IEEE Trans. Antennas Propag.*, vol. 65, no. 12, pp. 7257–7265, Sep. 2017.

[47] A. Basir, M. Zada, Y. Cho, and H. Yoo, "A dual-circular-polarized endoscopic antenna with wideband characteristics and wireless biotelemetric link characterization," *IEEE Trans. Antennas Propag.*, vol. 68, no. 10, pp. 6953–6963, Oct. 2020.

[48] K. Liu *et al.*, "Design of conformal spiral dual-band antenna for wireless capsule system," *IEEE Access*, vol. 9, pp. 117349–117357, 2021, doi: 10.1109/ACCESS.2021.3106735.

[49] R. Li and Y. Guo, "A conformal UWB dual-polarized antenna for wireless capsule endoscope systems," *IEEE Antennas Wireless Propag. Lett.*, vol. 20, no. 4, pp. 483–487, Apr. 2021, doi: 10.1109/LAWP.2021.3054676.

[50] D. Nguyen *et al.*, "An ultra-miniaturized antenna using loading circuit method for medical implant applications," *IEEE Access*, vol. 9, pp. 111890–111898, 2021, doi: 10.1109/ACCESS.2021.3103827.

[51] Y. Feng, S. P. Pan, J. W. Li, P. Chen, and G. S. Li, "Design of ultra-wideband conformal capsule antenna for wireless capsule endoscopy system," in *Proc. Cross Strait Radio Sci. Wireless Technol. Conf. (CSRSWTC)*, Fuzhou, China, Dec. 2020, pp. 1–3, doi: 10.1109/CSRSWTC50769.2020.9372442.

[52] S. Hayat, S. A. A. Shah, and H. Yoo, "Miniaturized dual-band circularly polarized implantable antenna for capsule endoscopic system," *IEEE Trans. Antennas Propagat.*, vol. 69, no. 4, pp. 1885–1895, Apr. 2021, doi: 10.1109/TAP.2020.3026881.

[53] K. Shahverdi, S. Hashemi, S. Sarafan, and H. Cao, "Triple-band implantable antenna design for biotelemetry applications in MICS/ISM/Wi-Fi/Bluetooth bands," *Technologies*, vol. 10, no. 4, pp. 91, 2022, doi: 10.3390/technologies10040091

[54] D. Nikolayev, A. K. Skrivervik, J. S. Ho, M. Zhadobov, and R. Sauleau, "Reconfigurable dual-band capsule-conformal antenna array for in-body bioelectronics," *IEEE Trans. Antennas Propag.*, vol. 70, no. 5, pp. 3749–3761, May 2022, doi: 10.1109/TAP.2021.3138264.

[55] Ö. F. Çelik, and B. S. Cumhur, "Compact triple-band implantable antenna for multitasking medical devices," *J. Electr. Eng.*, vol.73, no.3, pp.166–173, Jul. 2022, doi: 10.2478/jee-2022-0022

[56] S. S. Mosavinejad, P. Rezaei, A. A. Khazaei, and J. Shirazi, "A triple-band spiral-shaped antenna for high data rate fully passive implantable devices Author links open overlay panel," *Int J Electron Commun.*, vol. 159, p. 154474, 2023, doi: 10.1016/j.aeue.2022.154474.

[57] Y. A. Kamel, H. A. Mohamed, H. ELsadek, and H. M. ELhennawy, "Miniaturized Triple-band circular-polarized implantable patch antenna for bio-telemetry applications," *IEEE Antennas Wirel. Propag. Lett.*, vol. 22, issue 1, pp. 74–78, Jan. 2023, doi: 10.1109/LAWP.2022.3202310.

[58] Z. Bao, "Comparative study of dual-polarized and circularly-polarized antennas at 2.45 GHz for ingestible capsules," *IEEE Trans. Antennas Propag.*, vol. 67, no. 3, pp. 1488–1500, Mar. 2019, doi: 10.1109/TAP.2018.2888819.